Validation of a suite of codes for the structural response of vertical axis wind turbines

David Malcolm, December 2017

Table of Contents

List of figures

List of tables

1 Introduction

The vertical axis wind turbine was "re-invented" in 1970 by Peter South and Raj Rangi [1] of the Canadian National Research Council, Ottawa, where much development was carried out. Considerable development was also carried out at Sandia National Laboratories, New Mexico, especially into the structural dynamics of the curved Darrieus rotor [2, 3]. It was determined that the rotating frame effects of Coriolis action, rotational softening, and pretensioning played important roles.

The structural analysis at Sandia made use of the finite element code, NASTRAN, which at that time ran on main frame computers only and for which the cost was considerable. When personal computers became available later in the 1980s, it was natural to consider duplicating the capabilities of NASTRAN on the PC [4]. There were several challenges to this task: the RAM storage of early PCs was extremely limited (typically less than 1 MB); and the processors were several orders of magnitude slower than modern machines. For those reasons it was decided to use a modal approach to reduce the number of degrees of freedom. Such a step would not be necessary nowadays (the larger number of physical degrees of freedom could be accommodated) but the modal approach gives useful insight into the operating natural modes, and the aerodynamic loading and response. The theoretical background of this approach is described in [5].

1.1 Objectives

The objective of this document is to present data validating the predictions of the PC-based codes. This is done by comparisons with other codes and by comparison with field data.

2 Outline of codes

There are two principal codes: the EOLE code for extracting the operating natural frequencies and mode shapes, and the Forced Response (FR) code for determining the response to aerodynamic harmonic loading. Both codes make use of a shared finite element model of the rotor using beam elements only. The analysis is carried out relative to the rotating frame and assumes that the elastic restraints to this frame are axisymmetric. The relationship of the codes with their respective input and output files is shown in Figure 1.
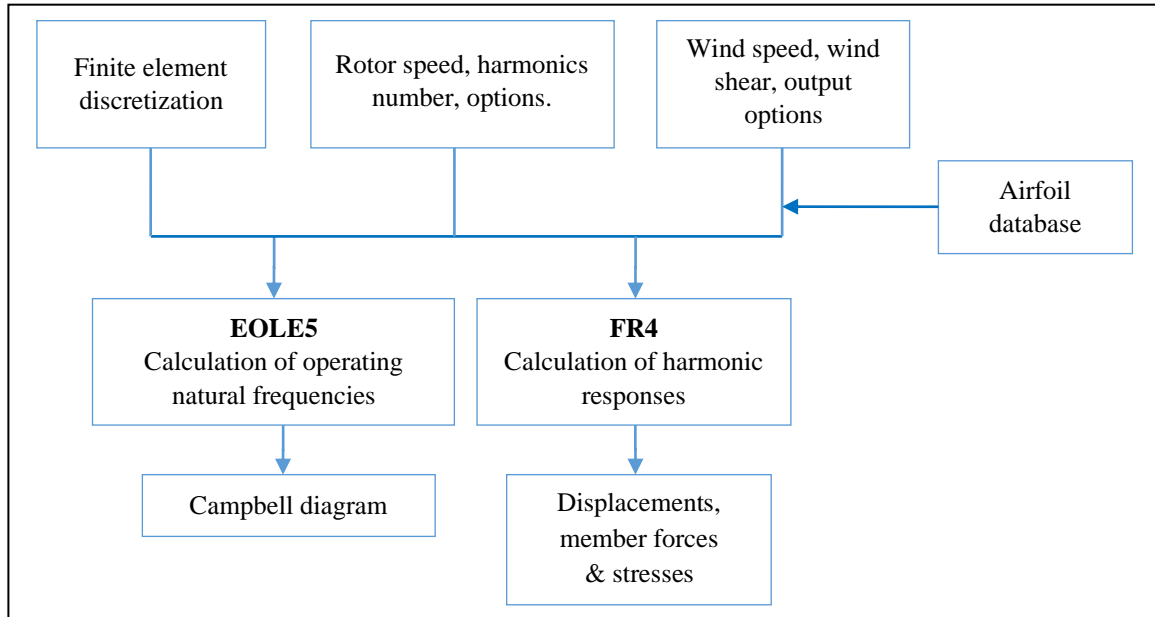
Figure 1. Flowchart of the EOLE suite of codes

3 Comparison with Sandia's codes

In 1993 the staff at Sandia National Laboratories carried out a comparison of the operating natural frequencies obtained for the Flowind 3-bladed, 23-m Darrieus rotor using both their own Nastran-based procedure and the FR4 code from D. Malcolm Associates. The comparison is summarized in Table 1, which is extracted from a report from T.D. Ashwill of SNL to Vern Wallace of Flowind Corporation [6].

Table 1. Comparison of natural frequency predictions from Nastran and EOLE4 for the Flowind 23-m Darrieus rotor

| Mode shape | 0 rpm | | 30 rpm | | 47 rpm | | 60 rpm | |
	Nastran	EOLE4	Nastran	EOLE4	Nastran	EOLE4	Nastran	EOLE4
	Hz	Hz	Hz	Hz	Hz	Hz	Hz	Hz
1Pr	0.144	0.144	0.148	0.141	0.152	0.138	0.157	0.134
1T1/BE	0.978	0.976	0.846	0.848	0.652	0.653	0.460	0.461
1T2/BE	0.98	0.98	1.04	1.041	1.095	1.095	1.144	1.14
1F1	1.246	1.243	1.583	1.572	1.874	1.855	2.017	2.00
1F2	1.25	1.247	1.591	1.58	1.902	1.881	2.138	2.11
1F3	1.259	1.256	1.61	1.599	1.958	1.94	2.229	2.2
TT1/BE	1.662	1.647	1.361	1.359	1.329	1.326	1.339	1.333
TT2/BE	1.664	1.675	2.132	2.132	2.415	2.415	2.53	2.523
2Pr	2.473		2.641		2.55		2.624	
2F1	2.548		2.781		3.203		3.613	
2F2	2.554		3.026		3.416		3.728	
2F3	2.579		3.042		3.45		3.798	

The following abbreviations are used to describe the mode shapes

1Pr	first propeller mode
F1, 1F2, 1F3	first flatwise modes
1Tl/BE, IT2/BE	first tower modes (with blade edgewise deformation)
2Fl, 2F2, 2F3	second flatwise modes

| 2Pr | second propeller mode |
| TTI/BE, TT2/BE | first tower modes with top motion (and blade edgewise deformation) |

The EOLE4 natural frequencies can be seen to agree well with corresponding values from the Nastran-based procedure. The latter has been compared with field data from several Darrieus rotors as part of the Sandia VAWT program.

4 Comparison with WHI field data

In 2015 Wind Harvest International (WHI) started testing a small straight-bladed VAWT at the Folkecenter site in Denmark. A general assembly drawing of this turbine is shown in Figure 4.

4.1 Operating natural frequencies

The stationary rotor was tested for its fundamental natural frequency which was found to be approximately 0.65 Hz. The finite element model within EOLE5 and FR4 was tuned to agree with this value.

4.1.1 Campbell diagram

The Campbell diagram for this turbine was obtained from the EOLE5 code and is shown in Figure 2 below. It predicts a 0P instability at approximately 42 rpm.
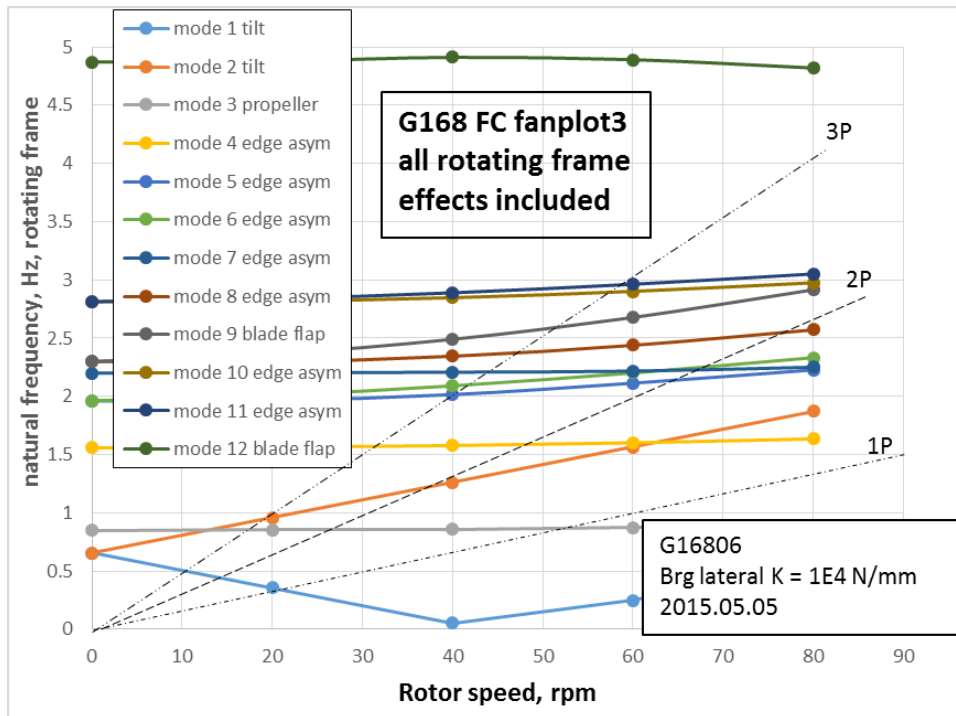

Figure 2. Campbell diagram for WHI G168 at Folkecenter, Denmark

4.1.2 0P resonance

Strain gauge data from the central mast were used to confirm the presence of the 0P resonance at approximately 42 rpm indicated on the Campbell diagram in Figure 2. During record 20160321-1201 the rotor speed fell from 50 rpm to as low as 43 rpm. When this happened the small out-of-balance inherent in the rotor was sufficient to superimpose a large steady bending on the central mast, as illustrated in Figure 3. From this it can be concluded that the resonant rotor speed is 43 rpm or lower. The turbine was

also operated at rotor speeds of up to 38 rpm without any 0P bending being observed. This implies that the resonance was above 38 rpm.
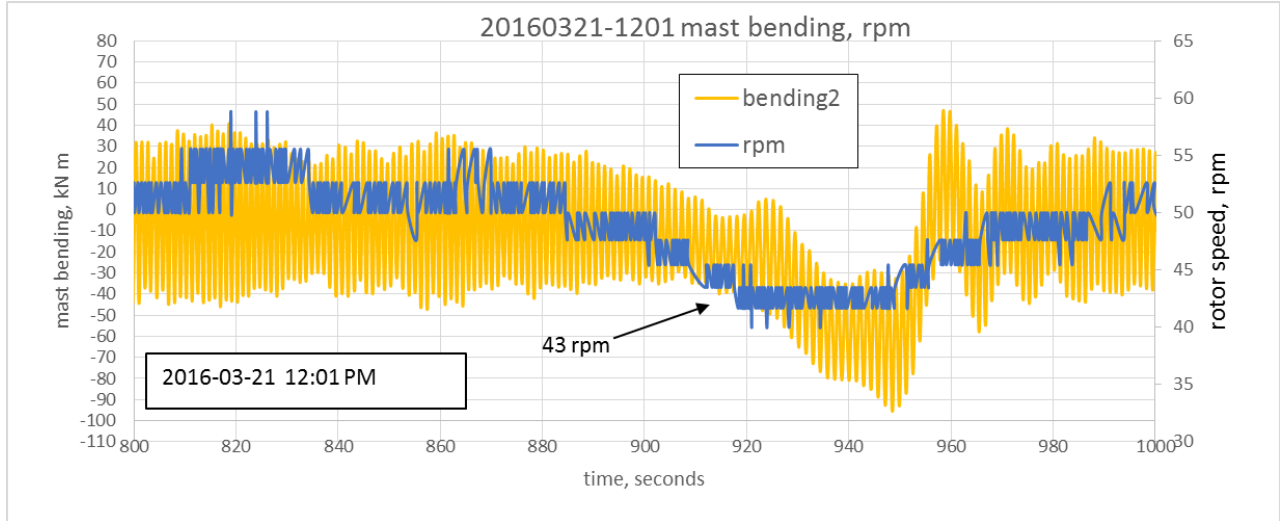

Figure 3. 0P resonance near 42 rpm

4.2   Operating forced response

The WHI G168 at the Folkecenter, Denmark, was fitted with strain gauges measuring both the bending in the central mast and flapwise bending in one of the blades. Details of the experimental configuration can be found in [8]. The location of the gauges is shown in Figure 4. Each of the mast bending gauges consisted of a full bridge and were calibrated by inserting a shunt resistor and by applying a measured external bending to the mast. The blade gauges (installed later) were placed at the maximum blade thickness and consisted of a half bridge.
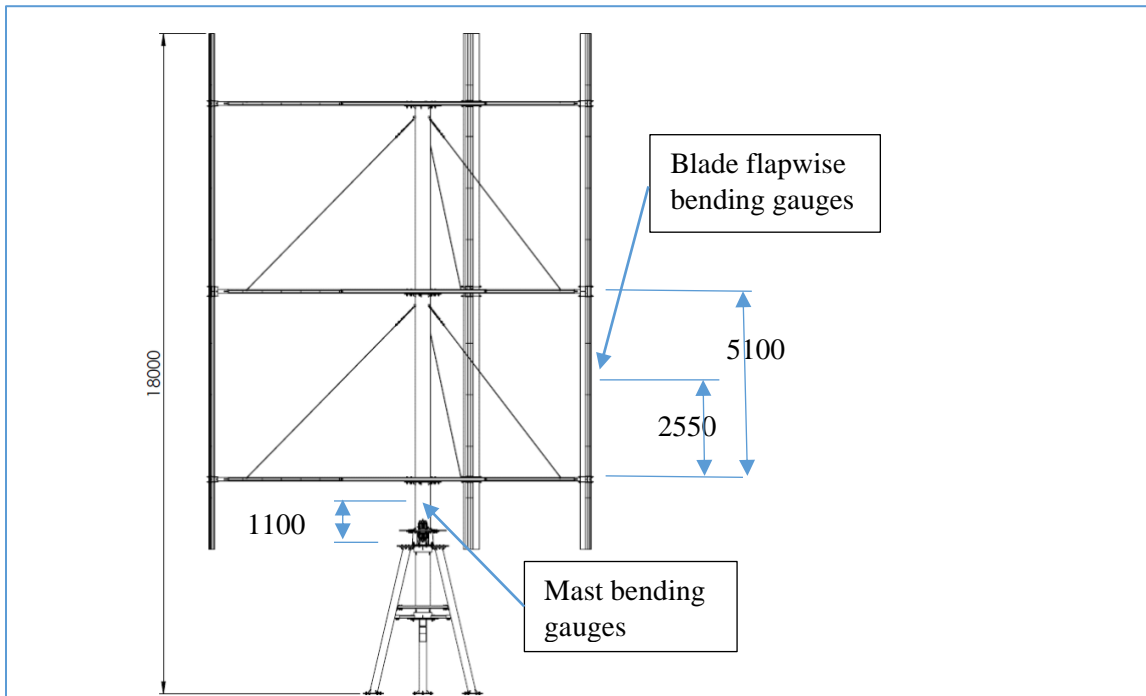

Figure 4. Location of strain gauges on WHI G168 at Folkecenter, Dk

Page 6

4.2.1   Mast bending, operation at 30-35 rpm

Mast bending data was collected on March 19th 2016 when the rotor speed was between 30 and 35 rpm and the average wind speed was approximately 8.2 m/s. A sample of the mast bending, the rotor speed, and the wind speed is shown in Figure 5.

Figure 5. Mast bending, wind speeds, and rotor speed, record 20190319-1312

There is a dominant 1P component in the mast bending signals but the amplitude of this component varies due to fluctuating wind speed and rpm values. To arrive at the most common excursion range in these signals (which is an indication of the average 1P component), the signals were processed by a rainflow algorithm [7]. Figure 6 shows the results of this process on 500 seconds of the signals
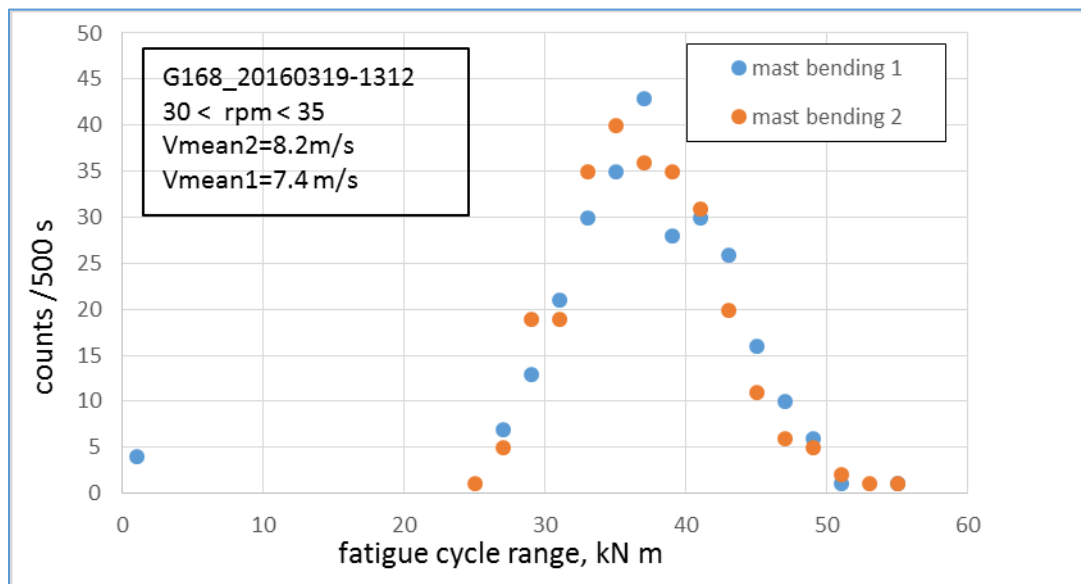
Figure 6. Rainflow counts of mast bending in record 20160319-1312

The rainflow counts indicate the most frequent magnitude (of the full range) to be between 35 and 40 kN m. This value was compared with the FR4 predictions using rotor speeds of 30 and 35 rpm and a wind speed of 8.2 m/s. The results are presented in Table 2.

Table 2. Summary of 1P bending ranges in field and model data, 30-35 rpm

	Rotor speed rpm	Wind speed m/s	Most frequent rainflow excursions kN m	1P range kN m
FR4 run 155, node 9	30	8.2		24
FR4 run 156 node 9	35	8.2		29
FR4 run xxx node 9	35	9.5		32
Field data 20160319-1312 200-700 s	Range: 30-35	Range:4-11 Mean 8.1	Upper 5%:35 – 40 Peak at 37	

Table 2 shows the range of FR4 predictions are somewhat less than the rainflow counts of the field data. The latter include the contributions from higher harmonics (2P and 3P) and might be expected to be slightly greater than the 1P alone.

4.2.2   Mast bending, operation at 50 rpm

Mast bending data were collected on March 21st 2016 when the rotor speed was between 50 and 53 rpm and the average wind speed was approximately 8.2 m/s. A sample of the mast bending, the rotor speed, and the wind speed is shown in Figure 7
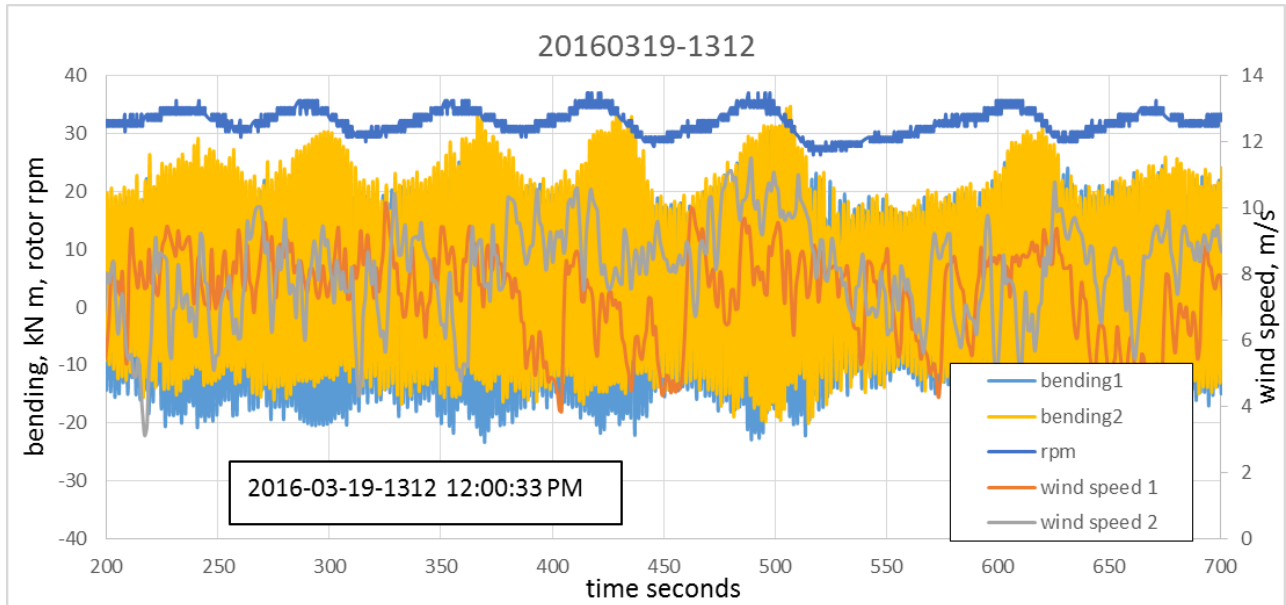

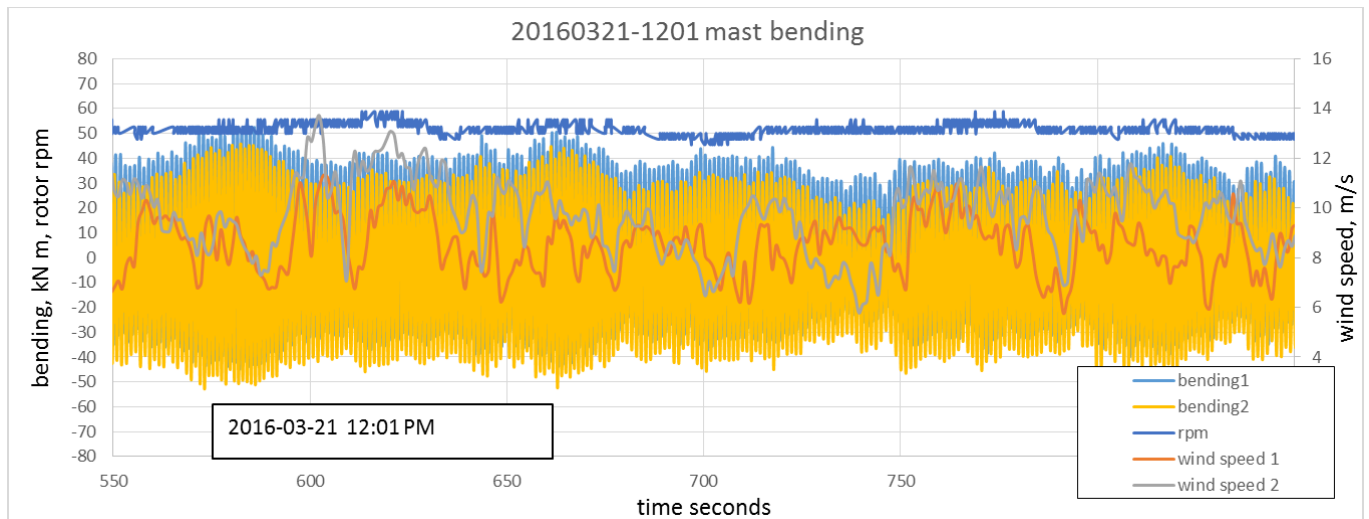Figure 7. Mast bending, wind speeds, and rotor speed, record 20190321-1201

Once again the amplitude of the dominant 1P component is masked by the variations in wind speed and, to a lesser extent, the rotor speed. To arrive at the most common excursion range in these signals, the signals were processed by a rainflow algorithm [7]. Figure 8 shows the results of this process on 300 seconds of the signals
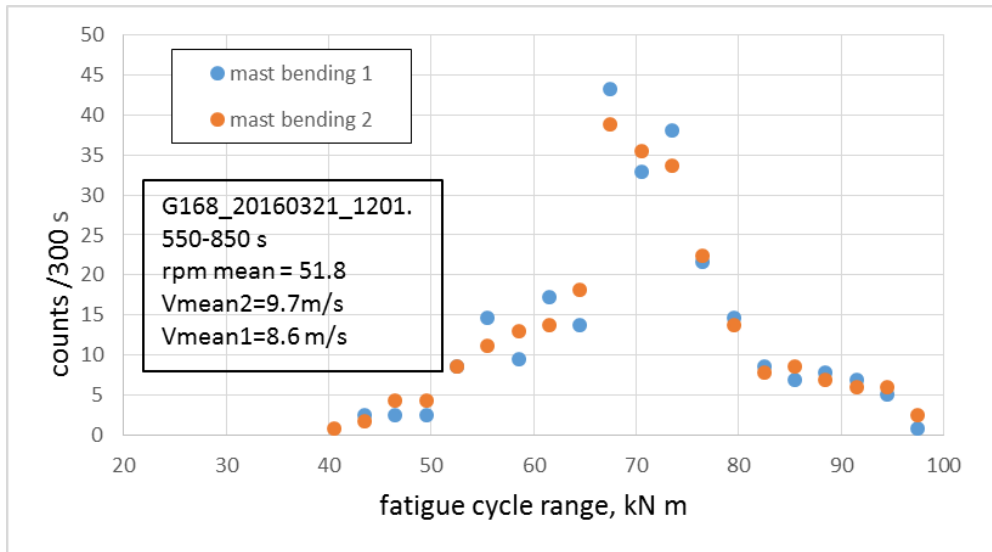
Figure 8. Rainflow counts of mast bending in record 20160321-1201

The rainflow counts indicate the most frequent magnitude (of the full range) to be between and 68 and 73 kN m. This value was compared with the FR4 predictions using rotor speeds of 50 and 52 rpm and a wind speeds of 8.6 and 9.0 m/s. The results are presented in Table 3

Table 3. Summary of 1P bending ranges in field and model data, 50-52 rpm

	Rotor speed rpm	Wind speed m/s	Most frequent rainflow excursions kN m	1P range kN m
FR4 run129 , node 9	52	9.0		96
FR4 run157 node 9	50	8.6		72
Field data 20160321-1201 550-850 s	Range: 48-53	Mean 9.7	Peak at 68- 73	

Table 3 shows the range of FR4 predictions overlaps well with the rainflow counts of the field data. The latter include the contributions from higher harmonics (2P and 3P) and might be expected to be slightly greater than the 1P alone.

4.2.3   Blade bending, operation at 30 rpm

A set of two gauges (making a half bridge) were installed in the center of a lower blade span in March 2016 (see Figure 4). Data were collected with an operating speed of between 30 and 38 rpm and a wind speed in the range of 10 to 15 m/s, as shown in Figure 9. The oscillations in the rotor speed are probably a function of the control system. The effects from centrifugal action can be noted from the changes in the mean bending relative to the stationary rotor. The effects of the aerodynamic loads are seen as the largely 1P cycles in the bending signal.

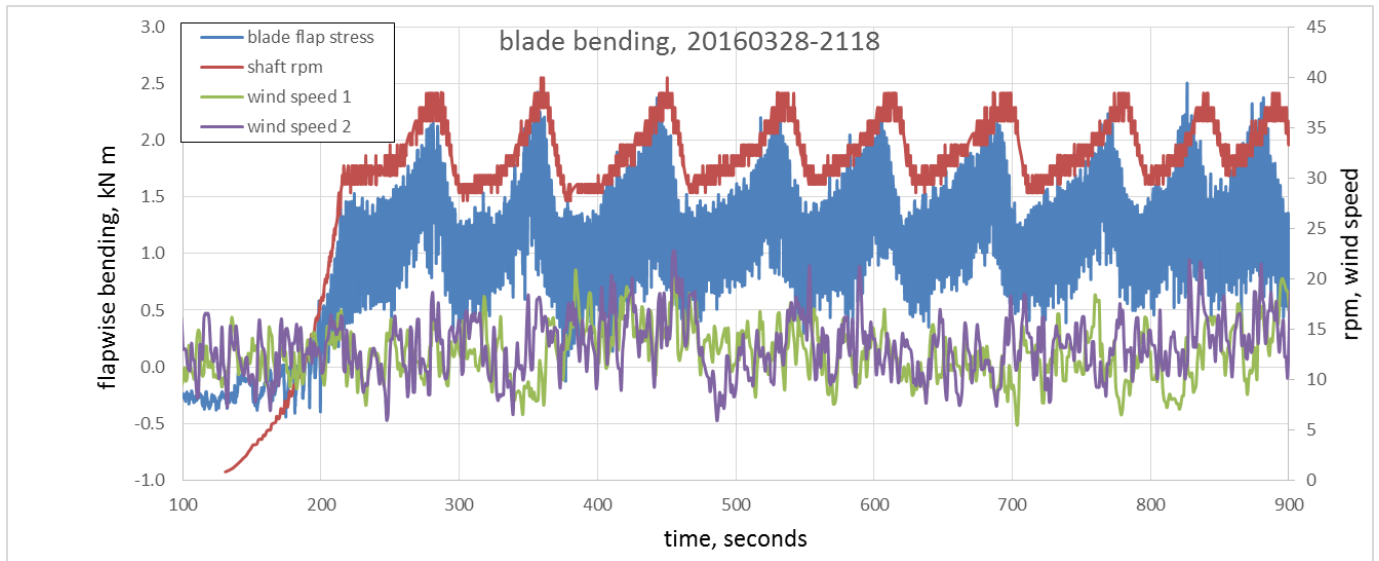Figure 9. Blade bending, rotor rpm, wind speed from record 20160328-2118

The bending signal was processed by a rainflow algorithm to identify the most common amplitude of these cycles which are shown in Figure 10. That figure suggests two values of peak frequency which are likely to be associated with the range of rotor speeds.
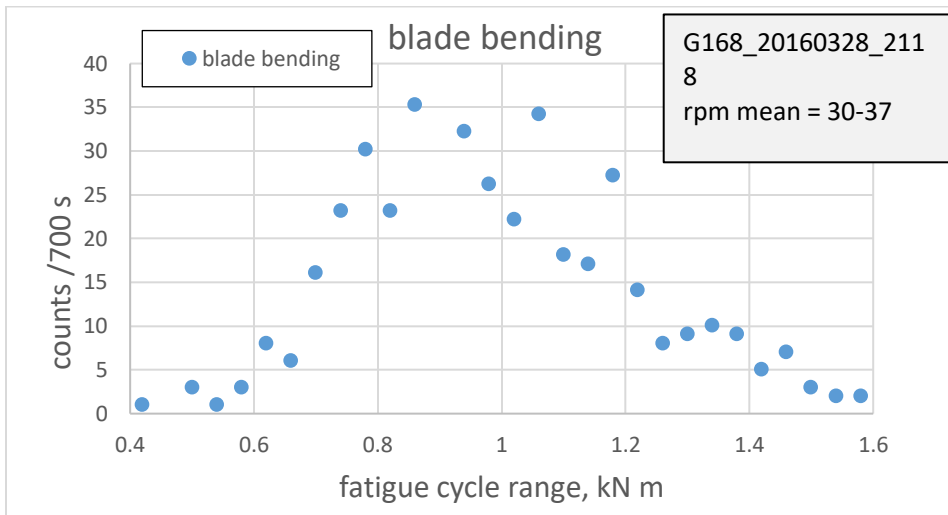

Figure 10. Distribution of rainflow counted excursions of flapwise bending

Table 4. Measured and predicted blade flapwise bending from centrifugal and from aerodynamic loads

rpm	Wind speed m/s	Centrifugal load estimate N/mm	Centrifugal bending FR4 estimate kN m	Centrifugal bending measured kN m	1P range FR4 estimate kN m	1P range measured kN m
30	14	0.716	1.64 run 153	1.40	0.96 run153	0.83
37	14	1.089	2.49 run 158	1.95	1.20 run158	1.03

4.2.4   Critical crossings

The Campbell diagram shown in Figure 2 includes a crossing of the 1P loading and the fundamental tilt mode at 20 rpm. It also shows a crossing of the 2P excitation with the fundamental tilt mode at 15 rpm. In the field, during the start-up procedure, some resonance was observed at 15 rpm but not at 20 rpm.

The FR4 code shows that the 1P loading consists largely of modal components of the first two (real) tilt modes with a 90° phase difference. These are also the two (real) modes that comprise the complex tilt mode shapes. However, the phase relationship of the two components in the complex mode are directly opposed to the phase relationship of the components of the 1P aerodynamic loading. This explains why no resonance was observed when the rotor speed passed through 20 rpm.

A similar analysis of the 2P crossing at 15 rpm showed that the modal components of the loading had the same phase relationship as the complex operating mode. Such a relationship leads to a potential resonance and a critical crossing which was confirmed by the field observations.

4.3   Summary

The Campbell diagram generated by the EOLE5 code predicted a 0P resonance at approximately 42 rpm. This was supported by field data for mast bending (see Figure 3)

Mast bending data during operation between 30 and 35 rpm (Figure 5) was compared to predictions from FR4. The field data was slightly greater than the model predictions

Mast bending data were also collected during operation between 50 and 52 rpm (Figure 7) and compared with FR4 model predictions. In this case the model predictions slightly exceeded the field data.

Flapwise blade bending data were collected during operation at 30-35 rpm and the values were compared with the FR4 model predictions. For both the centrifugal effects and for the response to aerodynamic loads the model predictions were approximately 15-20% greater than the field data. Possible reasons for this include:
- Both the rotor speed and the wind speed were not constant
- The strain gauges may not have been placed exactly at the position of maximum blade thickness.
- The section modulus of the blade may have been overestimated.

- The extent of restraint offered to the blade at the connection to the middle strut was uncertain. In the FR4 model the connection was assumed pinned whereas in practice it may have carried some moment.

The observed resonance when passing through 15 rpm and lack of any resonance when passing through 20 rpm was explained by an analysis of the modal phase relationships of the 1P and 2P aerodynamic loadings.

5　References

1. South, P. and R.S. Rangi. "Preliminary Test of a High Speed Vertical Axis Windmill Model," National Research Council of Canada, Ottawa, Ontario, March 1971.
2. Lobitz, D.W. "Forced Vibration Analysis of Rotating Structures with Application to Vertical Axis Wind Turbines," 5th Biennial Wind Energy Conference & Workshop (WWV) SERI/CP CONF-811043, Dept. of Energy, October 1981.
3. Lobitz, D.W. and Sullivan, W.N. "A Comparison of Finite Element Predictions and Experimental Data for the Forced Response of the DOE 100 kW Vertical Axis Wind Turbine," 6th ASES Biennial Wind Energy Conference and Workshop Proc, June 1983.
4. Malcolm, D.J. "VAWTFR: PC-FEM-BASED Program for Frequency Response of VAWTs," Sandia Wind Energy Project Contractor Review Meeting, Bushland, TX, May 1992.
5. Malcolm, D.J., "Theoretical basis of the Forced Response codes for Vertical Axis Wind Turbines", January 2016
6. Ashwill, T.D., Letter report to Vern Wallace of Flowind Corp concerning the structural analysis of the Flowind 23-m Darrieus rotor wind turbine, April 30, 1993
7. Socie, D.F., "Fatigue life predictions using local stress-strain concepts", Experimental Mechanics, Vol. 17, No. 2, February 1977
8. "A Proposal for Instrumentation on WHI's G168 v1.1 VAWT to be Installed in Canyon, Texas" Wind Harvest International, December 20176